ARTICLES

Nanosecond-to-femtosecond laser-induced breakdown in dielectrics

B. C. Stuart, M. D. Feit, S. Herman, A. M. Rubenchik, B. W. Shore, and M. D. Perry

Lawrence Livermore National Laboratory, P.O. Box 808, L-493, Livermore, California 94550

(Received 9 February 1995; revised manuscript received 4 October 1995)

We report extensive laser-induced damage threshold measurements on dielectric materials at wavelengths of 1053 and 526 nm for pulse durations τ ranging from 140 fs to 1 ns. Qualitative differences in the morphology of damage and a departure from the diffusion-dominated $\tau^{1/2}$ scaling of the damage fluence indicate that damage occurs from ablation for $\tau \lesssim 10$ ps and from conventional melting, boiling, and fracture for $\tau > 50$ ps. We find a decreasing threshold fluence associated with a gradual transition from the long-pulse, thermally dominated regime to an ablative regime dominated by collisional and multiphoton ionization, and plasma formation. A theoretical model based on electron production via multiphoton ionization, Joule heating, and collisional (avalanche) ionization is in quantitative agreement with the experimental results.

I. INTRODUCTION

Theoretical and experimental investigations of the pulse width and wavelength scaling of laser-induced damage in dielectrics have been the subject of numerous studies.[1–24] For pulses longer than a few tens of picoseconds, the generally accepted picture of bulk damage to defect-free dielectrics involves the heating of conduction-band electrons by the incident radiation and transfer of this energy to the lattice. Damage occurs when the deposited heat is sufficient to melt, boil, or fracture the dielectric material. Because the controlling rate is that of thermal conduction through the lattice, this model predicts[1,4] a $\tau^{1/2}$ dependence of the threshold damage fluence upon pulse duration τ. This is in reasonably good agreement with numerous experiments,[14–24] which have observed a τ^x scaling with nominally $0.3 < x < 0.6$ in a variety of pure and multilayer dielectric materials (including samples with defects) from 20 ps to over 100 ns.

Recently, the application of chirped-pulse amplification[25] (CPA) to solid-state lasers has enabled the construction of multiterawatt class systems that produce subpicosecond pulses. These systems are used routinely for investigations of high peak-power laser-matter interactions, such as coherent x-ray generation, relativistic plasma physics, and inertial confinement fusion.[26] Further increases in the peak power available from such systems are now limited by damage to optical surfaces, due to the intense short pulses.

A deviation from the long-pulse scaling of the breakdown threshold was first reported by Soileau *et al.*[18] for pulses in the range of 4–10 ps, and more recently by Du *et al.*[23] with pulses down to 150 fs. Here, we report extensive measurements of laser-induced damage thresholds, for pulse durations ranging from 140 fs to 1 ns, for fused silica and alkali fluorides. In each of these large-band-gap materials, we observe a change in the damage mechanism and morphology for pulses shorter than 20 ps. Although we observe a deviation from the long-pulse $\tau^{1/2}$ scaling, we find no evidence for the dramatic increase in damage threshold when the pulse width is decreased from 10 ps to 150 fs, as reported by Du *et al.*[23] Instead, we observe[24] a continuously decreasing threshold associated with a gradual transition from the long-pulse, thermally dominated regime, to an ablative regime dominated by collisional and multiphoton ionization, and plasma formation.

Our theoretical picture of laser-induced damage to dielectrics is much simpler for pulse durations less than about 10 ps than for longer pulses. In this short-pulse regime, intensities corresponding to breakdown produce electrons via photoionization, and these electrons initiate the avalanche. Indeed, as the femtosecond regime is reached, breakdown intensities approach the limit in which multiphoton ionization alone is capable of producing electron densities high enough (plasma critical density) to cause damage. The strong nonlinear dependence of multiphoton rates on intensity causes the threshold to become increasingly sharply defined for shorter pulse durations. Because there are no statistical fluctuations in the number of starting electrons, we are able to define the intrinsic damage threshold of the material. More importantly, for very short laser pulses, energy is absorbed by the electrons much faster than it is transferred to the lattice. Since the lattice does not heat appreciably during the pulse, there is no modification of electron-lattice scattering rates. There is also no need to track the flow of energy into the lattice to account for thermal and mechanical stresses, as is necessary with long ($\tau > 50$ ps) pulses.

A great deal of theoretical and empirical information exists on electron scattering in fused silica,[27,28] which we use in an empirically based model of the damage threshold. This model, with no adjustable parameters, is in good agreement with our measurements in the short-pulse regime and over a range of laser wavelength. Our results are also consistent with the temporally and spatially resolved measurements of surface plasmas in dielectrics by von der Linde and Schüler,[29] and the space-time observation of an electron gas produced by multiphoton absorption in SiO_2 reported by Audebert *et al.*[30]
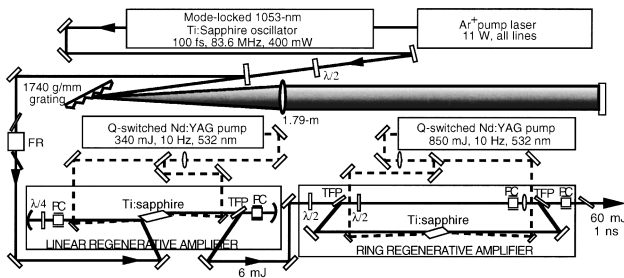
FIG. 1. Schematic diagram of a 1053-nm Ti:sapphire laser system, which produces 60-mJ, 1-ns stretched pulses at 10 Hz with better than 3% rms stability. PC—Pockels cell; TFP—thin-film polarizer; FR—Faraday rotator.

II. EXPERIMENT

For damage testing, we used laser pulses generated by a 1053-nm Ti:sapphire CPA system[31] (Fig. 1). Seed pulses of 100 fs from a Kerr-lens mode-locked, Ti:sapphire oscillator were stretched to 1 ns in a four-pass, single-grating pulse stretcher. Amplification by nearly 10^9 to the 6-mJ range was achieved in a TEM_{00} linear regenerative amplifier. We were careful to limit the energy extraction from this stage in order to avoid complications associated with self-phase modulation of the stretched, chirped pulse.[31,32] Further amplification to the 60-mJ level was achieved in a Ti:sapphire ring regenerative amplifier, which supported a larger mode and reduced nonlinear effects. This system operated at 10 Hz.

After amplification, we compressed the pulses in a four-pass, single-grating compressor of variable length (Fig. 2). By varying the dispersive path length of the compressor, we obtained pulses of continuously adjustable duration from 0.4 to 1 ns (all reported pulse widths are intensity full width at half maximum). Pulse durations were measured with a single-shot autocorrelator[33] (0.4–1.5 ps), streak camera (10–1000 ps), and fast photodiode (0.1–1 ns), and were calibrated against the linear position of the fold mirrors. The temporal profile of the compressed pulses depends strongly on the spectral and temporal profile of the stretched pulse.
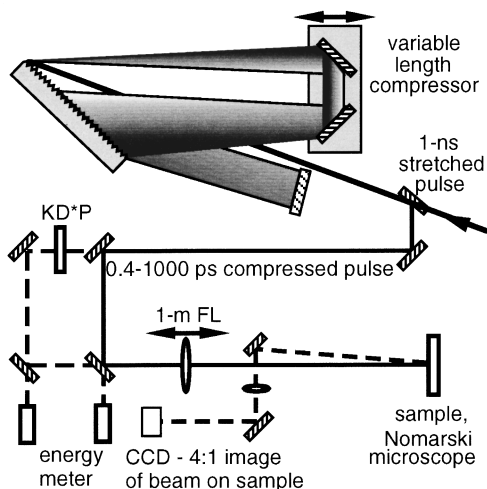

FIG. 2. The 1-ns stretched pulses are compressed to 0.4–1000 ps by a variable length compressor. A 1-m lens focuses the pulse on the sample and the spot size is measured with a 4:1 image. Frequency doubling creates 526-nm pulses down to 275 fs.

Pulse compression with spectral clipping is analogous to diffraction from a hard-edge aperture in the spatial domain, and results in a modulated temporal profile in the "intermediate" range of compression. For these damage measurements, we compressed a near-Gaussian spectral profile to obtain temporally smooth output pulses. This allowed us easily to relate the time evolution of the pulse intensity to the measured fluence.

We also measured damage thresholds with 526-nm light generated by frequency doubling the 1053-nm compressed pulses in a thin (4-mm) deuterated potassium dihydrogen phosphate (KD*P) crystal. The conversion efficiency was kept below 25% to avoid any temporal distortion of the second-harmonic pulse. We measured our shortest 526-nm pulses with a single-shot autocorrelator to be 275 fs. This was in good agreement with the expected $\sqrt{2}$ scaling from the 1053-nm pulse width, so this scaling was used for the other 526-nm pulse widths. Data was also taken at 825 nm and 140 fs, with a Cr:LISAF CPA system,[34] to confirm the decreasing trend in damage fluence with pulse width.

The energy of each pulse was monitored with the leakage through a 92% reflectivity mirror. We adjusted the energy delivered to the damage sample with a half-waveplate before compression. The rms energy stability was typically less than 3%, and we report the average value here. We performed damage measurements with laser spot sizes adjustable from 0.3- to 1.0-mm diameter (e^{-2} intensity). The typical diameter used was 0.5 mm, with 0.3 mm used to reach the higher threshold fluences required by the longer pulse lengths. Laser pulses were focused onto the damage sample by a 1-m focal length lens, with a variable distance to the sample. The spot size was measured on a charged coupled device (CCD) camera. With the shortest pulses that we used, the intensity (up to 4×10^{12} W/cm^2 on sample) became high enough to cause significant (10% effect) whole-beam self-focusing in the focusing lens and the air path leading to the sample. All beam size measurements were therefore performed with a 4:1 image of the beam taken from a 4% reflection at the position of the damage sample, and at or just below damage threshold. The laser mode at the sample had a 98% or better fit to a Gaussian, so the effective diameter, as measured on the camera system, was combined with the measured energy to give the pulse energy fluence. Our estimated absolute uncertainty in fluence was 15%, but relative values when changing the laser pulse width or spot size are accurate to 5%.

After irradiation, Nomarski microscopy was used to inspect the sample for possible damage. We define damage to be any visible permanent modification to the surface observable with the Nomarski microscope. The smallest damage spots that we could observe were approximately 0.5 μm in diameter, a factor of 10^6 smaller in area than the laser spot size and nearly impossible to observe by other methods (e.g., degradation of transmission, scattered light, etc.). To avoid the complications of spatial and temporal distortion caused by self-focusing, group-velocity dispersion, and self-phase modulation when propagating laser pulses through optical materials, we considered only front-surface damage. Depending on the focusing geometry and pulse duration, the rear surface or bulk of the transparent samples would often damage before the front surface, so we were careful not to let this damage propagate to the front surface.
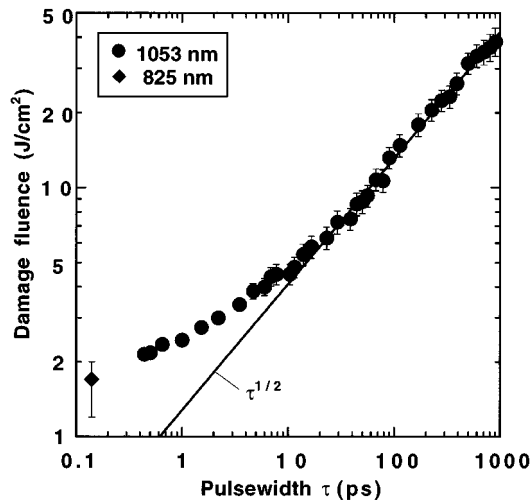
FIG. 3. Pulse width dependence of threshold damage fluence for fused silica.

Initial damage, at threshold, may have many forms: ablation of a very small amount of material (a few atomic layers); formation of a color center, shallow trap, or lattice defect; or melting of a very small volume. These weak effects are very difficult to detect after a single laser pulse. In order to "amplify" this damage to an easily observable size, and to minimize statistical uncertainty, we conducted our damage testing with multiple pulses of a given fluence on each site. This is in contrast to the single-shot measurements of Du et al.,[23] which required detection of plasma emission or a decrease in transmission caused by the single pulse. We typically used 600 shots at 10 Hz. Many fluence levels (15–30) were examined above and below the damage threshold for a given pulse width in order to establish the threshold value.

III. DAMAGE RESULTS

A. Fused silica

The results presented here for fused silica were obtained with 1-cm-thick "superpolished" samples (Corning 7940) exhibiting less than 1-nm rms surface roughness. We measured the same damage thresholds with a 200-μm-thick fused-silica etalon, which was tested to examine any possible differences between thick and thin samples. Some samples were cleaned initially with acetone or methanol, and all were cleaned when damage debris accumulated on the surface. No difference in threshold was found between samples or areas on a given sample that were or were not cleaned. Defects visible through the microscope were avoided. With short (0.4-ps) pulses, damage always occurred at the location corresponding to the peak of the Gaussian spatial profile, indicating that defect sites did not contribute to our measured thresholds. Ramping the fluence with short pulses, which would remove any surface contamination with lower threshold, gave the same damage threshold as our constant-fluence measurements. These results indicate that our measurements correspond to a uniform, defect-free surface and can be compared to calculations based on the intrinsic properties of fused silica. Further discussion of the role of defects and the influence of multiple pulses is given toward the end of the paper.
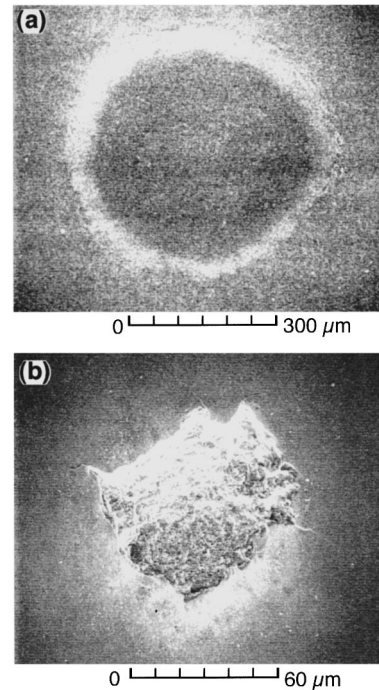

FIG. 4. Laser damage spots on fused silica created by (a) long pulse, 900-ps, 300-μm diameter; (b) short pulse, 0.4-ps, 500-μm diameter.

Our measured threshold damage fluence for fused silica at 1053 nm, as a function of laser pulse length [full width at half maximum (FWHM)] and a single point at 825 nm, are shown in Fig. 3. In the long-pulse regime ($\tau > 20$ ps), the data fit well to a $\tau^{1/2}$ dependence (actual fit: $\tau^{0.504}$), characteristic of transfer of electron kinetic energy to the lattice and diffusion during the laser pulse. The damage occurs over the en-
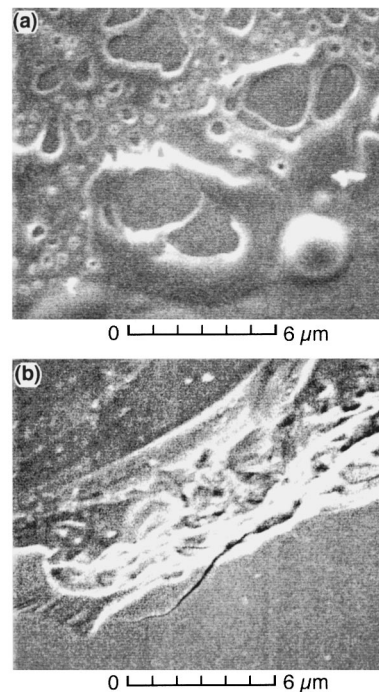

FIG. 5. Edges of laser damage spots of Fig. 4: (a) long pulse, 900 ps; (b) short pulse, 0.4 ps.
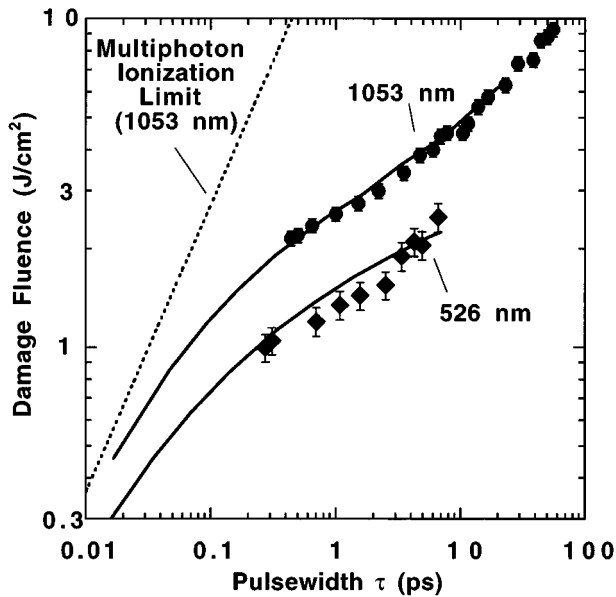
FIG. 6. Measured and calculated (solid lines) damage fluence for fused silica at 1053 and 526 nm. Dashed line indicates calculated damage limit, due to multiphoton ionization alone.

FIG. 7. Pulse width dependence of threshold damage fluence for calcium fluoride.

tire area irradiated, as shown in the electron micrograph of Fig. 4(a). (All damage micrographs shown are the result of multiple pulses.) The damage is thermal in nature and characterized by melting and boiling of the surface. This is more easily seen in Fig. 5(a), which shows the edge of the long-pulse damage spot. For pulses shorter than 20 ps, the damage fluence no longer follows the $\tau^{1/2}$ dependence and exhibits a morphology dramatically different from that observed with long pulses. Short-pulse damage is confined to a small region at the peak of the Gaussian irradiance distribution [Fig. 4(b)]. Damage occurs only over an area with sufficient intensity to produce ionization. With insufficient time for lattice coupling, there is no collateral damage. As a result, the damaged area can be many orders of magnitude smaller with short ($\tau < 10$ ps) pulses than with long pulses. For the case of fused silica shown in Fig. 4, the damaged area produced by the 0.5-mm diameter, 500-fs pulse was two orders of magnitude smaller than that produced by the 0.3-mm diameter, 900-ps pulse. Short-pulse damage appears as a shallow fractured and pitted crater characteristic of a thin layer of material removed by ablation [Fig. 5(b)]. We found damage in the short-pulse limit to be deterministic, with only a couple percent fluence range between damage and no damage. After determining the threshold fluence and leaving all other parameters fixed, we reduced the average energy delivered to the sample by 2%. The fused silica was irradiated with 10 000 pulses at several locations and showed no evidence of damage with 0.4-ps pulses. This shows experimentally, in the short-pulse limit, the lack of dependence of the damage threshold on defects or accumulation effects and the extremely sharp threshold resulting from multiphoton ionization. With long pulses (900 ps), there was an approximately 15% range in the damage threshold depending on position on the sample.

In Fig. 6, we concentrate on the short-pulse region and include our measured damage thresholds at 526 nm. The solid curves are the results of our theoretical modeling of laser-induced damage in the short-pulse limit (described be-
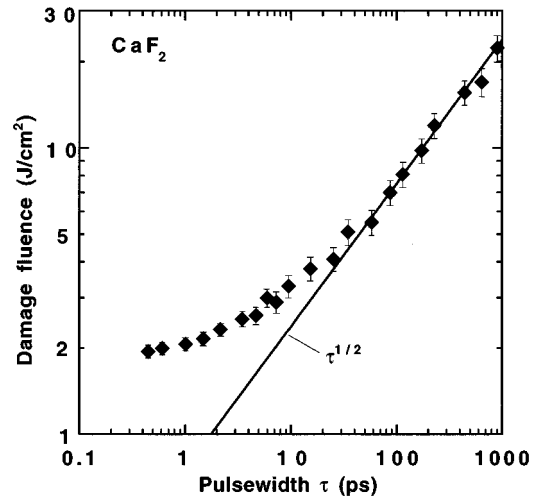
low), and are in very good agreement with both the *pulse width* and *wavelength* scaling of the measured data. In the modeling, we chose the plasma critical density ($\approx 10^{21}$ cm^{-3}) as the theoretical indicator of macroscopic damage. The calculated threshold is not sensitive to this choice; had we based our definition on an electron density of 10^{19} cm^{-3}, at which the energy density of conduction electrons equals the lattice binding energy, the threshold would decrease by approximately 20%. As shown and discussed below, with decreasing pulse width, the damage threshold will asymptotically approach the limit where multiphoton ionization alone creates sufficient electron density to cause damage.

B. Fluorides

The damage threshold of calcium fluoride exhibits a similar pulse width dependence as that of fused silica (Fig. 7). In the long-pulse limit, the threshold fluence also scales approximately as $\tau^{1/2}$, and then changes to the short-pulse limit near 20 ps. For long pulses, the damage morphology is again consistent with melting. Figure 8(a) shows the melting and recrystalization of the calcium fluoride surface layers, which occurred with no evidence of avalanche breakdown. This is consistent with the measurements in the long-pulse regime (100 ps) of Jones and co-workers[13,35] on wide-gap alkali halides. Short-pulse damage clearly initiates on scratches left from the polishing process [Fig. 8(b)], although as observed by Milam[36] with 125-ps pulses, the damage threshold did not appear to be greatly influenced by the polishing sleeks. Our measured short-pulse (0.4 ps) damage thresholds of BaF$_2$ (1.6 J/cm^2), CaF$_2$ (2.0 J/cm^2), MgF$_2$ (2.1 J/cm^2), and LiF (2.6 J/cm^2) scale with band-gap energy, as expected from multiphoton initiated avalanche ionization.

IV. THEORY OF ULTRASHORT-PULSE DAMAGE THRESHOLD

Optical breakdown in transparent materials is generally understood in terms of an electron avalanche[2,3,10,12,13] in which conduction-band electrons, oscillating in response to the laser field, transfer energy by scattering from phonons. If an electron can achieve an energy equal to the band gap,
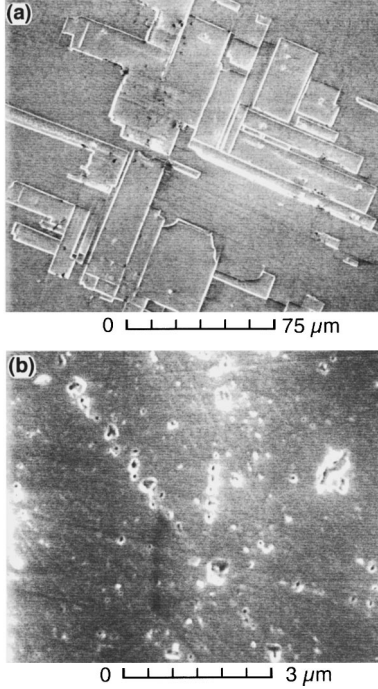
FIG. 8. Laser damage morphology of calcium fluoride for (a) 900-ps and (b) 0.4-ps pulses.

subsequent impact ionization promotes another valence electron into the conduction band. For long pulses (>10 ps), a delicate balance between electron energy gain and loss rates determines the breakdown threshold.

An adequate theoretical description of dielectric optical breakdown thresholds must answer three questions: First, what are the sources of the seed electrons that initiate the avalanche? Second, what are the rates for conduction-electron momentum and energy scattering? These rates determine the rate at which laser energy can be absorbed and, thus, the avalanche rate. Third, to what extent does significant heating of the lattice itself modify the scattering rates?

We have developed a general theoretical model of laser interaction with dielectrics in which very short intense pulses produce initial conduction-band electrons by multiphoton ionization. Because the pulses are so short, collisional heating of the electrons occurs before there is a significant transfer of energy from the electrons to the lattice. This heating and energy diffusion, combined with impact ionization, results in an electron avalanche, which is described by a kinetic equation. This is a classical approach, which in an average sense accounts for multiple-photon absorption by electrons in the conduction band.

We take the damage threshold to be indicated by the occurrence of a sufficiently high electron density. A reasonable lower limit would be on the order of 10^{19} cm^{-3}, roughly the density at which the energy density of conduction electrons equals the binding energy of the lattice. A more realistic choice is the critical electron density at which the plasma becomes reflective (10^{21} cm^{-3} for 1053 nm), since it is just below this density that the laser is strongly absorbed. Calculations indicate the theoretical threshold is only logarithmically dependent on this choice.

A. Kinetic equation

Our description of electron avalanche development is based on the solution of a kinetic equation for the electron distribution function. For insulators or other materials having a band-gap energy U_I large compared to the photon energy ($U_I \gg \hbar\omega$), the number density $f(\varepsilon,t)d\varepsilon$ of electrons with a kinetic energy between ε and $\varepsilon+d\varepsilon$ at time t is described by a Fokker-Planck equation,[3,10]

$$\frac{\partial f(\varepsilon,t)}{\partial t} + \frac{\partial}{\partial \varepsilon}\left[V(\varepsilon)f(\varepsilon,t) - D(\varepsilon)\frac{\partial f(\varepsilon,t)}{\partial \varepsilon}\right]$$

$$\equiv \frac{\partial f(\varepsilon,t)}{\partial t} + \frac{\partial J(\varepsilon,t)}{\partial \varepsilon} = S(\varepsilon,t), \tag{1}$$

where

$$V(\varepsilon) = R_J(\varepsilon,t) - U_{\text{phon}}\gamma(\varepsilon) = \frac{\sigma(\varepsilon)E^2(t)}{3} - U_{\text{phon}}\gamma(\varepsilon). \tag{2}$$

The current $J(\varepsilon,t)$ represents direct heating and loss, as well as an energy diffusion with coefficient $D(\varepsilon)$, which is proportional to both the conductivity and the laser intensity,

$$D(\varepsilon) = \frac{2\sigma(\varepsilon)E^2\varepsilon}{3}. \tag{3}$$

Here, ε is the electron energy, E is the electric field oscillating at frequency ω, U_{phon} is the characteristic phonon energy, R_J accounts for Joule heating of electrons in terms of the conductivity per electron $\sigma(\varepsilon)$,

$$\sigma(\varepsilon) = \frac{e^2\tau_m(\varepsilon)}{m^*[1+\omega^2\tau_m^2(\varepsilon)]}, \tag{4}$$

and $\gamma(\varepsilon)$ is the rate at which electron energy is transferred to the lattice. The quantity $1/\tau_m(\varepsilon)$ is the transport (momentum) scattering rate. Both $\tau_m(\varepsilon)$ and $\gamma(\varepsilon)$ are energy dependent, varying in fused silica by two orders of magnitude for energies in the conduction band.[28] The final term $S(\varepsilon,t)$ in Eq. (1) includes sources and sinks of electrons,

$$S(\varepsilon,t) = R_{\text{imp}}(\varepsilon,t) + R_{\text{pi}}(\varepsilon,t). \tag{5}$$

Impact ionization at rate R_{imp} was included assuming that excess kinetic energy is equally divided between the two resultant electrons,[3]

$$R_{\text{imp}}(\varepsilon,t) = -\nu_i(\varepsilon)f(\varepsilon) + 4\nu_i(2\varepsilon+U_I)f(2\varepsilon+U_I). \tag{6}$$

The ionization rate $\nu_i(\varepsilon)$ was taken in the Keldysh impact ionization form[37] as $1.5(\varepsilon/U_I-1)^2$ fs^{-1}. The factor of 4 in the second term of Eq. (6) can be justified by integrating Eq. (6) over energy. This shows that the net rate of electron production is simply $\int d\varepsilon\, \nu_i(\varepsilon)f(\varepsilon)$. The source term $S(\varepsilon,t)$ also includes multiphoton ionization at rate $R_{\text{pi}}(\varepsilon,t)$. The boundary conditions for Eq. (1) require the vanishing of the distribution at $\varepsilon=\infty$ and the current at $\varepsilon=0$.

Due to the rapid growth of the impact ionization rate for energies above the band gap, some researchers[10,12,13] have replaced the source term $R_{\text{imp}}(\varepsilon,t)$ in Eq. (6) by the boundary conditions,

$$f(U_I,t)=0; \quad J(0,t)=2J(U_I,t). \tag{7}$$

These conditions imply that every electron that reaches energy U_I generates a second electron by impact ionization and leads to two electrons at zero energy. The second of these is known as the "flux-doubling" condition. This formulation is advantageous if we assume exponential growth $\exp(\beta t)$ and replace $\partial f/\partial t$ by $\beta f(\varepsilon)$. The kinetic equation can then be replaced by an eigenvalue equation with β as the eigenvalue. We refer to this second formulation as the flux-doubling model. The equivalence of the two formulations depends on the impact ionization rate being much larger than the rate at which the band-gap energy is being absorbed. That is,

$$U_I \nu_i(2\varepsilon+U_I) \gg \sigma_{\max}E^2, \tag{8}$$

for small ε. For ultrashort intense pulses, this inequality no longer holds. For example, in fused silica at 1053 nm, $\sigma_{\max}E^2 = U_I\nu_i(1.5U_I)$ at an intensity on the order of 10 TW/cm^2. Thus, the equivalence of the two formulations cannot be taken for granted, but must be checked. Further development of the flux-doubling model is given below and in Appendix A. We use this model to develop an analytic estimate of the avalanche rate, which we compare to numerical simulations of the kinetic equation.

The important physical quantities n (electron number density) and $\langle\varepsilon\rangle$ (average kinetic energy per electron) are defined for the full kinetic equation by the moments,

$$n=\int_0^\infty f(\varepsilon)d\varepsilon, \tag{9}$$

and

$$n\langle\varepsilon\rangle=\int_0^\infty \varepsilon f(\varepsilon)d\varepsilon. \tag{10}$$

Ignoring photoionization for now, we see from Eqs. (1) and (6) that

$$\frac{\partial n}{\partial t}=\int_0^\infty \nu_i(\varepsilon)f(\varepsilon)d\varepsilon=\langle\nu_i\rangle n, \tag{11}$$

and

$$\frac{\partial(n\langle\varepsilon\rangle)}{\partial t}=\int_0^\infty\left[\left(\sigma+\frac{2}{3}\varepsilon\frac{\partial\sigma}{\partial\varepsilon}\right)E^2-U_{\text{phon}}\gamma\right]f(\varepsilon)d\varepsilon$$
$$-U_I\int_0^\infty\nu_i(\varepsilon)f(\varepsilon)d\varepsilon$$
$$=(\langle\sigma\rangle E^2-U_{\text{phon}}\langle\gamma\rangle-U_I\langle\nu_i\rangle)n. \tag{12}$$

The corresponding equations for the flux-doubling model are similar, except for the impact ionization term, which is replaced by the boundary conditions. Thus, we expect $J(0)$ to be smaller for the full kinetic equation than for the flux-doubling model.

Aside from the derivative of σ in Eq. (12), this equation looks formally like the simple Drude theory used to describe electron energy gain by Joule heating and loss by transfer to the lattice.[2] However, the effective transport coefficients involved, such as

$$\langle\sigma\rangle=\int_0^\infty\left(\sigma(\varepsilon)+\frac{2}{3}\varepsilon\frac{\partial\sigma(\varepsilon)}{\partial\varepsilon}\right)f(\varepsilon)d\varepsilon\left/\int_0^\infty f(\varepsilon)d\varepsilon\right., \tag{13}$$

depend on averaging over the non-Maxwellian distribution function $f(\varepsilon)$, which is yet to be determined. Note that when exponential avalanche growth occurs, the shape of $f(\varepsilon)$ remains unchanged and $\langle\sigma\rangle$ is time independent.

We can distinguish two different behavioral regimes. For low-intensity long-duration pulses, it is possible to have balance or near balance between the first two terms on the right-hand side of Eq. (12). In this case, the few initial electrons in the conduction band cannot gain enough energy to initiate an avalanche. The energy absorbed by these electrons from the external field is used not to create new electrons, but is transferred into the lattice. In this long-pulse regime, the source of the initial seed electrons can be local defects or impurities. For damage to occur, the temperature near the local absorption centers must be sufficiently high to cause fracture or melting. The rate limiting process for temperature growth has been interpreted to be lattice thermal diffusion, which is characterized[1,4] by the threshold fluence for damage being proportional to $\tau^{1/2}$ (see Fig. 3).

At high laser intensity, the energy absorbed from the laser field cannot be transferred to the lattice as fast as it is deposited in the electrons. In this case, the absorbed energy is used to feed the avalanche. The average energy per electron is high, but remains fixed. To estimate the bounding intensity, I_b, between the long- and short-pulse regimes, we use Eq. (12). Initially all electrons are concentrated near the bottom of the conduction band. In this case, the derivative term in Eq. (12) is small and $\sigma(\varepsilon)$ and $\gamma(\varepsilon)$ can be evaluated at zero energy. As a result, we have the condition for avalanche dominated regimes:

$$\sigma(0)E^2 > U_{\text{phon}}\gamma(0). \tag{14}$$

For parameters characteristic of fused silica, this gives $I_b \approx 80$ GW/cm^2. At 5 J/cm^2, this corresponds to a pulse length $\tau_b \approx 60$ ps, which is roughly the pulse width at which we observe a deviation from the long-pulse $\tau^{1/2}$ scaling (Fig. 3). Our calculations treat optical damage in fused silica for intensities, $I \gg I_b$, and pulse durations $\tau \ll \tau_b$. Under these conditions energy transfer to the lattice is small, hence, we may treat the temperature of the lattice as a constant and consider the functions $\sigma(\varepsilon)$ and $\gamma(\varepsilon)$ unchanged during the pulse.

B. Solutions of the kinetic equation

Electron scattering from various types of phonons determines the transport scattering and loss rates appearing in Eq. (1). It is currently not possible to construct a first-principles theoretical model of all these interactions. The best approach combines theoretical reasoning with experimental data about interaction constants, deformation potential, etc., to construct a semiempirical model. We used the results summarized by Arnold, Cartier, and DiMaria,[28] which give a good account of electron scattering in fused silica. We assumed $m^*=m_e$, $U_I=9$ eV, and the characteristic phonon energy, U_{phon} was
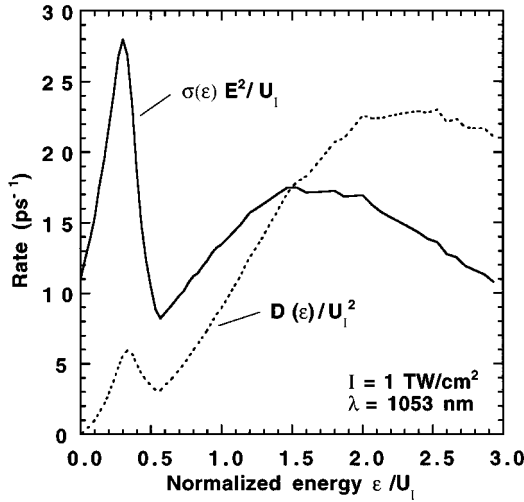
FIG. 9. Normalized conductivity and (energy) diffusion for conduction-band electrons. U_I is the band-gap energy.

taken as 0.033 eV. The resulting conductivity $\sigma(\varepsilon)$ and energy diffusivity $D(\varepsilon)$ are plotted in Fig. 9 as a function of electron energy.

The numerical solution of the kinetic equation at constant laser intensity and excluding multiphoton ionization shows that an avalanche is established within a few femtoseconds for an intensity of 1 TW/cm^2 (see Fig. 10). During the avalanche, the electron distribution grows in magnitude without changing shape, i.e.,

$$f(\varepsilon,t)=g(\varepsilon)\exp(\beta t). \qquad (15)$$

The distribution $g(\varepsilon)$ is stationary, but non-Maxwellian. The length of the initial transient is weakly dependent on initial conditions and decreases monotonically with increasing intensity. In the flux-doubling formulation, it can be shown (Appendix A) that for $I \gg I_b$,

$$\beta=pE^2 \left/ \int_0^{U_1} \frac{d\varepsilon}{\sigma(\varepsilon)} = \alpha I, \right. \qquad (16)$$
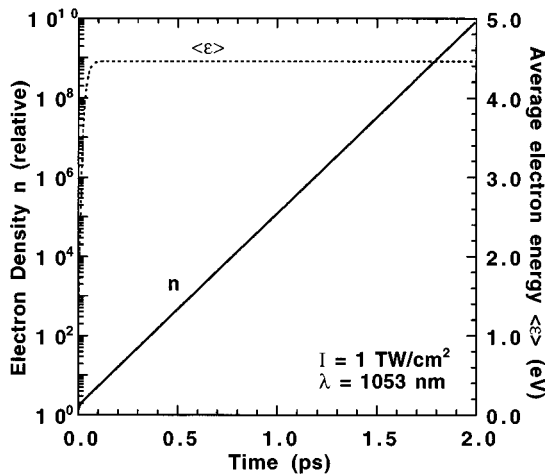

FIG. 10. Time dependence of the electron density n and average kinetic energy $\langle\varepsilon\rangle$ when subjected to a constant laser intensity. The electron density grows exponentially after a very short transient.
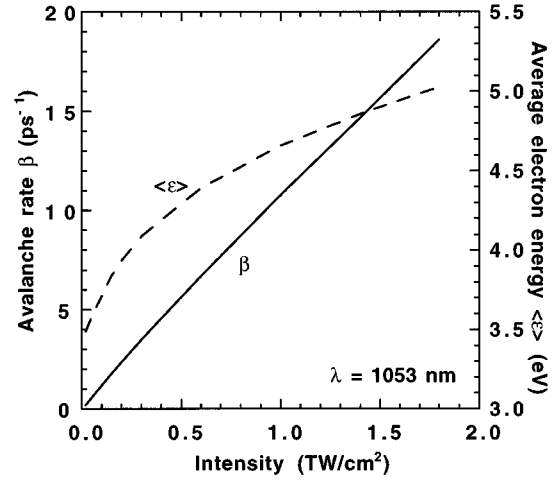

FIG. 11. Intensity dependence of the avalanche rate, β, and average electron energy $\langle\varepsilon\rangle$.

where p is a numerical factor between 0.5 and 1.0, and $I \propto E^2$ is the light intensity. At 1053 nm, Eq. (16) predicts that α has a value between 0.0065 and 0.013 cm^2/ps GW in useful units. More conventionally, $1/\alpha$ lies between 0.08 and 0.16 J/cm^2. This sets the scale for the damage fluence, as seen below. The linearity between β and intensity implied by Eq. (16) is borne out by our detailed calculations, as shown in Fig. 11.

The shortness of the transient solution for constant laser intensity suggests that for a time-varying pulse shape $I(t)$, we may expect a solution for the electron distribution function of the form $f(\varepsilon,t)=g(\varepsilon)\exp[\int \beta \, dt]$, with $\beta=\alpha I(t)$. This supposition is tested in Fig. 12, in which we plot the electron density as a function of the instantaneous fluence,

$$\Phi(t)=\int_{-\infty}^{t} I(t')dt', \qquad (17)$$

for the case of a Gaussian pulse. It is evident that the linearity between β and I holds throughout nearly the entire pulse.
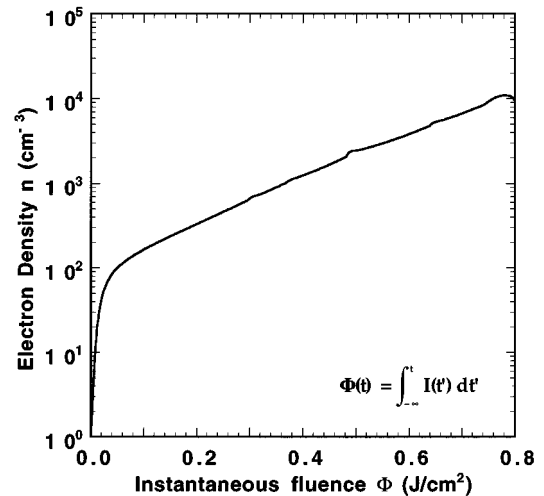

FIG. 12. With a time-varying (Gaussian) pulse, after a short transient the electron growth rate is proportional to the laser intensity. From this, we find the value of α.
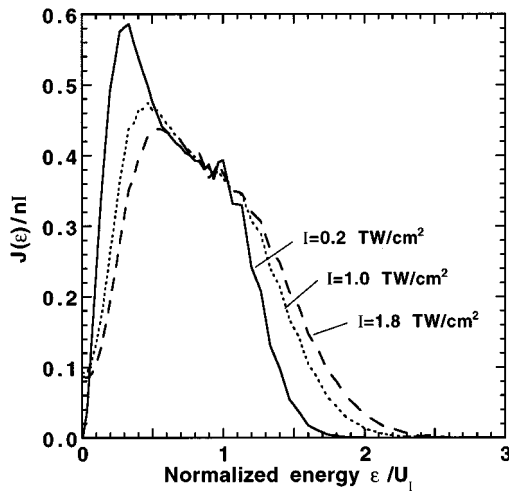
FIG. 13. Dependence of the current density $J(\varepsilon)$ on electron energy resulting from a numerical solution to the kinetic equation.

Strictly speaking, the scaling of the distribution function $f(\varepsilon)$ and current $J(\varepsilon)$ with intensity as well as the proportionality $\beta = \alpha I$ are assured only if the flux-doubling boundary conditions are valid. In addition, the average electron energy $\langle \varepsilon \rangle$ is independent of intensity under these conditions. The impact ionization terms in Eq. (6) formally spoil the scaling. However, the number of electrons with energy above U_I remains relatively small and there does not appear to be much effect on β. With impact ionization explicitly accounted for, $\langle \varepsilon \rangle$ increases with increasing intensity. Our numerical calculations, shown in Fig. 11, display the near linearity of β, with respect to I as expected from Eq. (16). From the figure, $\alpha = 0.011$ cm^2/ps GW, which is close to the flux-doubling value found earlier. The increase in average energy with increasing intensity is also evident.

As remarked above, both the distribution function $f(\varepsilon)$ and the current density $J(\varepsilon)$ would maintain invariant shapes, if exact scaling pertained. The intensity dependence of $J(\varepsilon)/nI$ for the full kinetic equation is not extremely strong, as is shown in Fig. 13. Note also the tail in the electron energy distribution, which extends well beyond the band-gap energy. The size of this tail depends on the relative rates of energy absorption and collisional ionization. With the proportionality between β and I, and the exponential growth of Eq. (15), the evolution of the electron density can be described by

$$\frac{dn}{dt} = \beta n = \alpha I(t) n. \qquad (18)$$

We now reintroduce multiphoton ionization $R_{\mathrm{pi}}(\varepsilon,t)$ in the source term $S(\varepsilon,t)$ of Eq. (1). This term is of the form $P(I)F(\varepsilon)$. Here, $P(I)$ is the multiphoton ionization rate and $F(\varepsilon)$ is the distribution function of the photoelectrons normalized, so that $\int F(\varepsilon)d\varepsilon = 1$. The photoionization process is sensitive to the Keldysh parameter,[38] $z = \omega(2mU_I)^{1/2}/eE$. For $z \gg 1$, which is the case here, the electron has time for many oscillations in the binding potential before being ionized.

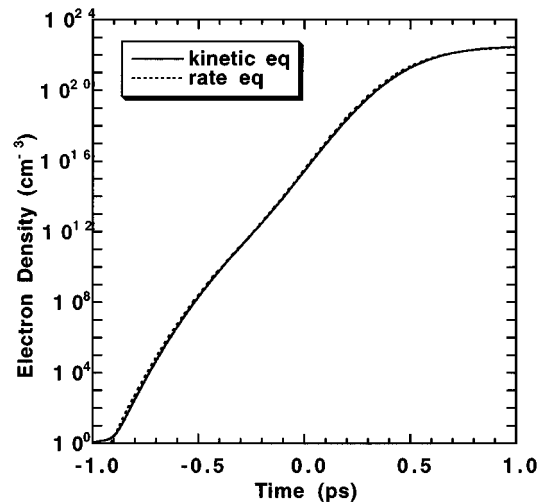For 526-nm light, four-photon absorption is the relevant process, and

FIG. 14. Comparison of solutions of full kinetic equation and corresponding rate equation for generation of critical density plasma with no seed electrons.

$$P(I) = \sigma_4 \left(\frac{I}{\hbar\omega} \right)^4 N_s. \qquad (19)$$

We used the cross section $\sigma_4 = 2 \times 10^{-114}$ cm^8 sec^3. This was measured for NaCl, but other insulators have nearly the same value.[13] The quantity N_s is the solid atom density. In any case, our results are not very sensitive to the exact numerical value of these rates.

For 1053-nm light, eight-photon absorption cross-section values were not available, so we used the strong-field Keldysh formula[38] for $P(I)$. Evaluation of the Keldysh expression leads to a result that is fit very well by the eight-photon absorption form.[39] We used the fit,

$$P(I) = 9.52 \times 10^{10} I^8 \quad \mathrm{cm}^{-3}\,\mathrm{ps}^{-1}, \qquad (20)$$

where the intensity I is in TW/cm^2. This expression should be valid up to intensities on the order of 10^3 TW/cm^2. For extremely short intense pulses, when $z \ll 1$, tunneling through the binding barrier takes place during a time shorter than the laser period. In this case, $P(I)$ can be taken as the Ammosov, Delone, and Krainov (ADK) tunneling ionization expression.[40]

The presence of photoionization perturbs the distribution function. However, if the transient time of Eqs. (11) and (12) is small in comparison with the typical time for electron density increase due to photoionization, the distribution function will remain close to $g(\varepsilon)$. Under these conditions, the avalanche development can be described by a simple rate equation,

$$\frac{\partial n}{\partial t} = \beta(I)n + P(I). \qquad (21)$$

Even for high photoionization rates, the rate equation can be justified as follows: The photoionization is strongly peaked at the center of the pulse. After the peak passes, photoionization becomes unimportant. The electrons produced at the peak serve as seed electrons for the avalanche. Hence, Eq. (21) can be considered as an interpolation scheme, which smoothly describes the transition between the

two extremes. Our numerical calculations confirm this picture. Figure 14 compares solutions of Eqs. (1) and (21) for a 1053-nm 1-ps Gaussian pulse with a peak intensity of 3.5 TW/cm^2. The close agreement between the two solutions justifies using the rate equation Eq. (21).

C. Determination of damage threshold

We will first present an analytic estimate of damage thresholds and scaling of thresholds by assuming that the two processes of multiphoton and avalanche ionization can be separated. Since multiphoton ionization is strongly peaked near the pulse maximum, the total number of electrons produced by a Gaussian pulse of duration τ (FWHM),

$$I(t) = I_0 \exp(-4 \ln 2 \, t^2/\tau^2), \tag{22}$$

is given approximately by

$$n = n_0 \exp\left[\int_0^\infty \beta \, dt \right] = n_0 \exp\left[\frac{\alpha I_0 \tau}{4} \left(\frac{\pi}{\ln 2} \right)^{1/2} \right], \tag{23}$$

where $n_0 = \int_{-\infty}^\infty P(I) dt$ is the total number of electrons produced by multiphoton ionization. The avalanche is assumed to start at the peak of the pulse. For example, at 526 nm, we have

$$n_0 = N_s \int_{-\infty}^\infty \sigma_4 \left(\frac{I(t)}{\hbar \omega} \right)^4 dt = \sigma_4 N_s \left(\frac{I_0}{\hbar \omega} \right)^4 \left(\frac{\pi}{\ln 2} \right)^{1/2} \frac{\tau}{4}. \tag{24}$$

The threshold fluence F_{cr}, corresponding to the density n_{cr} is then given by

$$F_{cr} = \frac{I_0 \tau}{2} \left(\frac{\pi}{\ln 2} \right)^{1/2} = \frac{2}{\alpha} \ln\left(\frac{n_{cr}}{n_0} \right). \tag{25}$$

The scale fluence $2/\alpha$ is 0.2 J/cm^2 for fused silica. The resulting threshold fluence is only logarithmically sensitive to the multiphoton cross section and the critical density.

One can also see from the form of Eq. (23), that if the number of seed electrons were independent of intensity, e.g., due to defects, the breakdown threshold F_{cr} would be independent of pulse duration. In the present case, n_0 increases rapidly with intensity, so that F_{cr} decreases as the pulse duration decreases, because the avalanche becomes less important. It is clear from Eq. (23) that avalanche ionization is not significant if the threshold fluence is such that $\alpha F_{cr}/2$ is small, i.e., F_{cr} of order 0.2 J/cm^2. Below this fluence, photoionization is almost completely responsible for dielectric breakdown. Indeed, since photoionization produces an ever increasing share of electrons for shorter pulse lengths, the short-pulse damage threshold must asymptotically approach the fluence at which photoionization alone produces the electron critical density n_{cr}. The threshold fluence for such short pulses will scale as

$$\Phi_{cr} = \tau^{3/4} \left(\frac{n_{cr}}{\sigma_4 N_s} \right)^{1/4} \left(\frac{\pi}{\ln 2} \right)^{3/8} \frac{\hbar \omega}{\sqrt{2}}, \tag{26}$$

for four-photon absorption, and more generally, as $\tau^{(m-1)/m} n_{cr}^{1/m}$ when m-photon ionization is the dominant process.
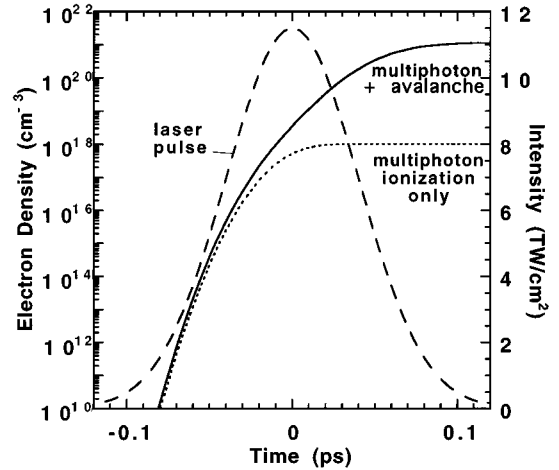

FIG. 15. Total (solid) and multiphoton produced (dotted) electron densities are plotted along with the Gaussian pulse shape. Seed electrons are produced by multiphoton ionization at the pulse peak after which an avalanche produces a critical density.

Returning now to solutions of the full time-dependent kinetic equation, Fig. 15 illustrates the evolution of electron density produced by a 100-fs, 12-TW/cm^2 pulse incident on fused silica. The pulse intensity and the electron density produced by photoionization alone are included for reference. Because photoionization is extremely intensity dependent, the electron production takes place principally at the peak of the pulse. After these "seed" electrons are produced, a small electron avalanche achieves a critical density plasma. It is important to note that the dense plasma is not produced until late in the pulse. Only this last part of the pulse experiences strong absorption or reflection. Note that we expect thresholds to be more sensitive to the pulse shape for longer pulses, where the avalanche is relatively more significant.

The above numerical values all pertain to the wavelength 1053 nm. At first glance, one would expect a strong frequency dependence in the avalanche rate, because of the denominator of Eq. (4). The maximum value of $\omega \tau_m$ at 526 nm is about 1.4. However, this value occurs at low energy which, as remarked earlier, is relatively ineffective at determining the value of β. Instead, according to Eq. (16), it is the minimal values of $\sigma(\varepsilon)$, the bottleneck, that determine the avalanche rate. The denominator $(1 + \omega^2 \tau^2)$ in Eq. (4) is nearly equal to unity at these values, so that we do not expect a strong frequency dependence. Indeed, our numerical calculations lead to the value $\alpha = 0.013$ cm^2/ps GW and a scale fluence $(2/\alpha)$ of 0.15 J/cm^2 for fused silica at 526 nm.

Figure 6 compares our theoretical values for short-pulse damage thresholds in fused silica with our measured values at 1053 and 526 nm. The agreement of both the *pulse width* and *wavelength* scaling is excellent, and is an indication that we are indeed measuring the intrinsic damage threshold of our fused silica samples.

D. Propagation

In order to ascertain where in the sample the plasma formation and short-pulse laser damage actually occurs, we next consider the amount of plasma created during damage and the depth of penetration of the laser pulse. Pulse propagation into the medium is governed by the continuity equation,

$$\frac{\partial W_e}{\partial t} + \frac{\partial I}{\partial z} = 0, \tag{27}$$

where $\partial W_e / \partial t$ is the rate per unit volume of energy deposition from the laser pulse into the electrons given by the Joule heating rate,

$$\frac{\partial W_e}{\partial t} = \langle \sigma \rangle n E^2. \tag{28}$$

Rearranging Eq. (12), we see that

$$\langle \sigma \rangle n E^2 = \frac{\partial}{\partial t} \left(n[\langle \varepsilon \rangle + U_I] \right) + \langle \gamma \rangle U_{\mathrm{phon}} n. \tag{29}$$

During an avalanche, the average electron energy $\langle \varepsilon \rangle$ is time independent and the electron density grows exponentially as described by Eq. (18). Thus, Eq. (29) can be written as

$$\langle \sigma \rangle n E^2 = (\alpha I[\langle \varepsilon \rangle + U_I] + \langle \gamma \rangle U_{\mathrm{phon}}) n, \tag{30}$$

which expresses the fact that energy absorbed by the electrons is used either to create more electrons via impact ionization or is passed to the lattice. Combining Eqs. (27), (28), and (30) with

$$\frac{\partial I}{\partial z} = -aI, \tag{31}$$

we identify the intensity absorption coefficient as given by the expression,

$$aI = (\alpha I[\langle \varepsilon \rangle + U_I] + \langle \gamma \rangle U_{\mathrm{phon}}) n. \tag{32}$$

For sufficiently high intensities (short-pulse limit), this simplifies to the result,

$$a = \alpha n[\langle \varepsilon \rangle + U_I], \tag{33}$$

which is directly proportional to the avalanche coefficient α of Eq. (18) and the electron density n. The absorption depends on intensity through $\langle \varepsilon \rangle$, but the proportionality to electron number density n is far more significant.

We can estimate the absorption coefficient at 1053 nm, by taking $\alpha^{-1} = 0.1$ J/cm^2 and $\langle \varepsilon \rangle + U_I = 15$ eV. This gives $a = 2.4(n/n_{\mathrm{cr}})$ μm^{-1}, where n_{cr} is the critical density, 10^{21} cm^{-3}. That is, near the critical density, the absorption length is on the order of a wavelength. This implies that for a pulse just above the damage threshold, a thin layer of dense plasma will be formed at the tail end of the pulse.

This layer will be even thinner as the material fully ionizes at intensities above threshold. To treat this case, we need to make two generalizations of the above description. First, since dense plasmas can strongly reflect laser light, this effect has to be accounted for when breakdown occurs before the end of the pulse. Second, once full ionization is reached, the absorbed energy of Eq. (28) is no longer used to collisionally ionize further electrons, but rather is used to increase the average energy per electron.

The optical response of the electron plasma is given by the complex Drude dielectric function,

$$\varepsilon(\omega) = 1 - n \frac{\langle \sigma \rangle}{\omega} (i + \omega \tau_m) = 1 - \frac{n}{n_c} \frac{1}{(1 + i/\omega \tau_m)}. \tag{34}$$
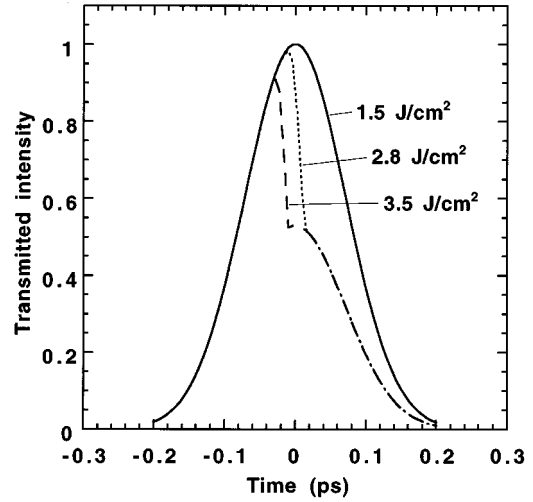

FIG. 16. Effect of reflection at the electron plasma boundary on the transmitted pulse shape of initially Gaussian 166-fs pulses. The pulse fluences are 1.5 (solid), 2.8 (dotted), and 3.5 J/cm^2 (dashed), respectively. The highest fluence is more than twice the threshold value.

The imaginary part of $\varepsilon(\omega)$ determines the absorption coefficient and corresponds to Eq. (33), i.e., the absorption by electrons is proportional to the conductivity. The intensity transmission at the plasma boundary can then be found from the Fresnel formulas as

$$T = \left| \frac{2 \operatorname{Re} \sqrt{\varepsilon(\omega)}}{1 + \sqrt{\varepsilon(\omega)}} \right|^2. \tag{35}$$

Figure 16 illustrates the effect of this interfacial reflection on the pulse shape just inside the plasma boundary. The initial pulse width is 166 fs and the curves have been normalized to their peak intensities for ease of comparison. Near threshold (1.5 J/cm^2), very little reflection occurs since high electron densities are not reached until very late in the pulse. Above threshold, however, there is a strong effect as the plasma reflects a significant fraction of the incident pulse. Note that the transmission does not vanish for the dense plasma, because $\omega \tau_m < 1$ in Eq. (34), i.e., the plasma is collisional.

Once full ionization is reached at the surface, further energy absorption heats a very thin layer of electrons. In Fig. 17, the cumulative energy deposited in fused silica is shown for the three pulses of Fig. 16, as a function of depth from the surface. Near breakdown threshold (1.5 J/cm^2), the laser-pulse energy absorbed by the plasma is distributed over many wavelengths, the deeper deposition corresponding to earlier parts of the pulse. On a molecular scale, energy deposition takes place well into the bulk and thus the breakdown corresponds to intrinsic properties of the material. The energy deposition is not so deep, however, that we have to worry about self-focusing or self-phase modulation over this short distance. At intensities above threshold, once high electron density is reached, all further deposition occurs in a thin skin depth. Considering that approximately one quarter of the 3.5-J/cm^2 input pulse energy is reflected, the deposition of 62% of this energy within the first micrometer is quite striking. Looking at the propagation in another way, Fig. 18
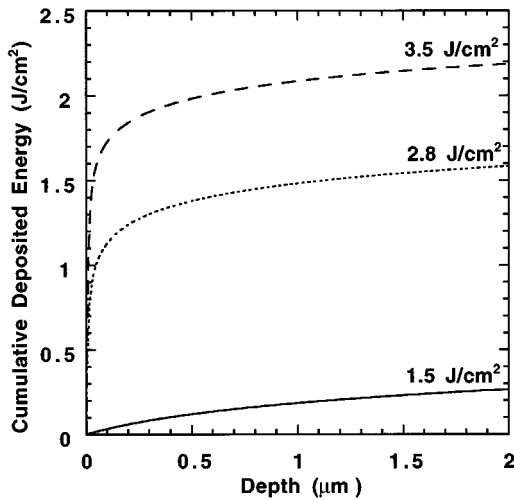
FIG. 17. Cumulative laser energy initially deposited in the electrons for the three pulses of Fig. 16. Above threshold, a significant fraction of the input pulse energy is deposited in a skin depth much thinner than a wavelength.

shows the electron density near the surface at fluences of approximately half, one, and two times breakdown threshold for the 166-fs pulse. Formation of a thin skin depth is evident in the above-threshold curve. The huge decrease in density at only half threshold shows the dramatic contribution of multiphoton ionization, which leads to our observation of an extremely sharp threshold.

E. Influence of defects and multiple pulses

In relatively pure dielectrics, the importance of initial concentrations of defect or impurity provided electrons for long-pulse damage is eliminated for short pulses. To see this, consider the simplified model of electron density growth [Eq. (21)] in the case of a temporally flat pulse, so that the coefficients are independent of time. The exact solution for this equation is
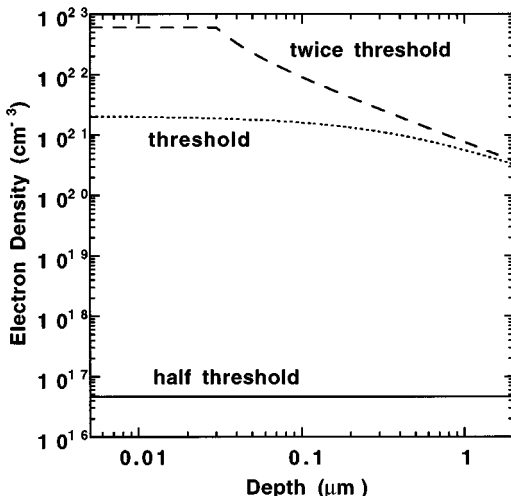
FIG. 18. Calculation of the electron density as a function of depth from the fused silica surface at fluences of roughly half, one, and two times the threshold for a 166-fs pulse.

$$n(t) = \left(\frac{P}{\beta} + n_0\right) \exp(\beta t) - \frac{P}{\beta}, \qquad (36)$$

where n_0 is the initial electron concentration. Equation (36) shows that the multiphoton ionization rate P is equivalent to an initial electron density. When multiphoton ionization contributes substantially more electrons than initially present ($P/\beta \gg n_0$), the growth of the electron density during the laser pulse becomes independent of the initial electron concentration. Since the m-photon ionization rate scales with intensity as I^m, and the avalanche rate β scales as I, the effective initial concentration scales as I^{m-1} and is quite large for our short intense pulses. For example, at an intensity of 10 TW/cm^2, an initial electron concentration less than about 10^{17} cm^{-3} is unimportant. Similarly, a concentration of 10^8 cm^{-3} (used as the "lucky electrons" in some avalanche theories) in fused silica will be important only for pulses longer than approximately 5 ps, otherwise the electron contribution from multiphoton ionization will dominate. We, therefore, believe that our measurements in the short-pulse regime (<10 ps) correspond to the intrinsic properties of the material, whereas thresholds measured with longer pulses are influenced by the presence of defects.

This independence of initial electron concentration for short-pulse damage means that moderate production of defects in multiple-pulse measurements does not change the monopulse evolution or breakdown threshold. Instead, the damage due to a single pulse is simply scaled to a more visible size by the succeeding pulses. As we have shown, the critical density plasma at threshold is reached only at the tail end of the laser pulse. This plasma, because of its initiation by multiphoton ionization, is highly localized. The localization implies faster cooling of the plasma for shorter pulse lengths. This makes the determination of damage threshold from plasma effects (decrease in pulse transmission, plasma emission, etc.) from a single short (<1 ps) pulse increasingly difficult. When the pulse width is increased, the mechanism of damage changes as initial defects and coupling of energy to the lattice during the pulse play increasingly important roles. The use of multiple pulses (succeeding pulses become part of the diagnostic) serves to amplify single-pulse damage to a easily observable size. These sensitivity effects may account for the observed apparent increase in breakdown threshold with a decreasing pulse width of Du et al.[23]

Another important practical issue is the presence of surface cracks, nodules, or voids, since such features are known to increase the local-field intensity by a factor of η^4, where η is the refractive index.[2] This increase takes place over a region comparable to the feature scale length, and is offset by convection of electrons away from the region. A simple estimate of convection shows that for picosecond pulses the local enhancement is insignificant for feature scale lengths less than 40 nm. Our super-polished fused silica sample exhibited less than 1-nm rms surface roughness.

V. SUMMARY AND CONCLUSIONS

We have investigated the pulse width dependence of laser-induced damage in pure and multilayer dielectrics over the range 0.1–1000 ps. We observe a strong deviation of laser damage fluence from the long-pulse $\tau^{1/2}$ scaling. This devia-

tion occurs for pulses shorter than 20 ps, below which electrons have insufficient time to couple to the lattice during the laser pulse. The damage threshold continues to decrease with decreasing pulse width, but at a rate slower than $\tau^{1/2}$ in the range 0.1–20 ps. This departure is accompanied by a qualitative change in the damage morphology indicative of rapid plasma formation and surface ablation. Due to the strong intensity dependence of multiphoton ionization, we find that damage caused by subpicosecond pulses is characterized by localized ablation, with essentially no collateral damage. Many applications, ranging from materials processing to biomedical technologies, will benefit from the more localized energy deposition of short-pulse lasers, as compared to long-pulse lasers.

A theoretical model with no adjustable parameters, in which initial electrons provided by multiphoton ionization are further heated resulting in collisional (avalanche) ionization, predicts short-pulse damage thresholds in excellent quantitative agreement with both the pulse width and wavelength dependence of our measurements for fused silica. The ablation takes place from a thin layer at the dielectric surface, but still well within the bulk material, so that we are measuring the intrinsic properties of the material. This is further justified by the relative insignificance of defects in the short-pulse limit. For extremely short pulses ($\tau < 40$ fs), multiphoton ionization alone can provide the critical density of electrons to cause damage. Our theoretical analysis of laser-induced breakdown in the short-pulse regime can be extended to any dielectric material for which the complex index of refraction, band gap, electron-scattering rates, and photoionization cross section are known.

ACKNOWLEDGMENTS

APPENDIX A: FLUX-DOUBLING MODEL

The flux-doubling model consists of Eq. (1), with $S(\varepsilon,t)=0$ together with the flux-doubling boundary conditions of Eq. (7). We wish to evaluate the electron avalanche rate β. Previous theoretical estimates[10] have been made for constant scattering rates, or by assuming vanishingly small β. Neither of these assumptions is valid in the short-pulse

limit. Moreover, the calculation assuming small β used perturbation theory based on the solution of the steady-state equation $\partial J/\partial\varepsilon=0$, which violates the flux-doubling boundary condition, $J(0)=2J(U_I)$. Hence, the applicability of this result[10] is not clear.

To evaluate β, we will employ the equation for the current J found by differentiating the eigenvalue equation,

$$\frac{\partial J}{\partial\varepsilon}=-\beta g(\varepsilon), \qquad (A1)$$

with respect to energy. Here, $g(\varepsilon)$ is defined in Eq. (15). This gives

$$D(\varepsilon)\frac{d^2J}{d\varepsilon^2}-V(\varepsilon)\frac{dJ}{d\varepsilon}=\beta J, \qquad (A2)$$

with D and V, as defined in Eq. (1) and with boundary conditions

$$J(0)=2J(U_I) \quad \text{and} \quad \frac{\partial J}{\partial\varepsilon}=0 \quad \text{at} \quad \varepsilon=U_I. \qquad (A3)$$

From Eq. (A1), one can conclude that J is a monotonically decreasing function of the energy, changing from $2J(U_I)$ to $J(U_I)$ within the conduction band. For high laser intensity, when losses to the lattice are negligible, Eq. (A2) can be rewritten as

$$\frac{d^2J}{d\varepsilon^2}-\frac{1}{2\varepsilon}\frac{dJ}{d\varepsilon}=\frac{\beta J}{D(\varepsilon)}. \qquad (A4)$$

Multiplying Eq. (A4) by ε integrating over energy, and applying the boundary conditions of Eq. (A3), we have

$$\frac{3}{2}J(U_I)=\beta\int_0^{U_I}\frac{J(\varepsilon)\varepsilon\ d\varepsilon}{D(\varepsilon)}. \qquad (A5)$$

Substituting the maximum and minimum values for the flux J into Eq. (A5) gives

$$\beta=\frac{pE^2}{\int_0^{U_I}\dfrac{d\varepsilon}{\sigma(\varepsilon)}}, \qquad (A6)$$

where $p=0.5$ or 1, corresponding to the limiting values of J. Our numerical calculations indicate a value of $p=0.85$. We see in Fig. 13 that realistic treatment of impact ionization modifies the structure of $J(\varepsilon)$ near the bottom of the conduction band. Fortunately, the ε weighting of the numerator in the integral of Eq. (A5) means that low-energy values are relatively unimportant in determining β.

[1] E. S. Bliss, Opto-electronics **3**, 99 (1971).

[2] N. Bloembergen, IEEE J. Quantum Electron. **QE-10**, 375 (1974).

[3] L. H. Holway, Jr. and D. W. Fradin, J. Appl. Phys. **46**, 279 (1975).

[4] J. R. Bettis, R. A. House II, and A. H. Guenther, Natl. Bur. Stand. (U.S.) Spec. Publ. **462**, 338 (1976).

[5] A. S. Epifanov, A. A. Manenkov, and A. M. Prokhorov, Zh. Eksp. Teor. Fiz. **70**, 728 (1976) [Sov. Phys. JETP **43**, 377 (1976)].

[6] W. L. Smith, J. H. Bechtel, and N. Bloembergen, Phys. Rev. B **15**, 4039 (1977).

[7] A. Schmid, P. Kelly, and P. Bräunlich, Phys. Rev. B **16**, 4569 (1977).

[8] B. G. Gorshkov, A. S. Epifanov, and A. A. Manenkov, Zh. Eksp. Teor. Fiz. **76**, 617 (1979) [Sov. Phys. JETP **49**, 309 (1979)].

[9] A. Vaidyanathan, T. W. Walker, and A. H. Guenther, IEEE J.

Quantum Electron. **QE-16**, 89 (1980).

[10] M. Sparks, D. L. Mills, R. Warren, T. Holstein, A. A. Maradudin, L. J. Sham, E. Loh, Jr., and D. F. King, Phys. Rev. B **24**, 3519 (1981).

[11] R. M. Wood, *Laser Damage in Optical Materials* (Hilger, Boston, 1986).

[12] A. A. Manenkov and A. M. Prokhorov, Usp. Fiz. Nauk **148**, 179 (1986) [Sov. Phys. Usp. **29**, 104 (1986)].

[13] S. C. Jones, P. Braunlich, R. T. Casper, X.-A. Shen, and P. Kelly, Opt. Eng. **28**, 1039 (1989).

[14] E. S. Bliss, D. Milam, and R. A. Bradbury, Appl. Opt. **12**, 677 (1973).

[15] E. W. Van Stryland, M. J. Soileau, A. L. Smirl, and W. E. Williams, Phys. Rev. B **23**, 2144 (1981).

[16] W. H. Lowdermilk and D. Milam, IEEE J. Quantum Electron. **QE-17**, 1888 (1981).

[17] T. W. Walker, A. H. Guenther, and P. E. Nielsen, IEEE J. Quantum Electron. **QE-17**, 2041 (1981); **QE-17**, 2053 (1981).

[18] M. J. Soileau, W. E. Williams, E. W. Van Stryland, T. F. Boggess, and A. L. Smirl, Natl. Bur. Stand. (U.S.) Spec. Publ. **669**, 387 (1984).

[19] S. R. Foltyn and L. J. Jolin, Natl. Inst. Stand. Technol. Spec. Publ. **752**, 336 (1988).

[20] J. H. Campbell, F. Rainer, M. Kozlowski, C. R. Wolfe, I. Thomas, and F. Milanovich, Proc. SPIE **1441**, 444 (1991).

[21] K. Mann, H. Gerhardt, G. Pfeifer, and R. Wolf, Proc. SPIE **1624**, 436 (1992).

[22] S. V. Garnov, A. S. Epifanov, S. M. Klimentov, and A. A. Manenkov, Proc. SPIE **1848**, 403 (1993).

[23] D. Du, X. Liu, G. Korn, J. Squier, and G. Mourou, Appl. Phys. Lett. **64**, 3071 (1994).

[24] B. C. Stuart, M. D. Feit, A. M. Rubenchik, B. W. Shore, and M.

[25] D. Strickland and G. Mourou, Opt. Commun. **56**, 219 (1985); P. Maine, D. Strickland, P. Bado, M. Pessot, and G. Mourou, IEEE J. Quantum Electron. **24**, 398 (1988).

[26] M. D. Perry and G. Mourou, Science **264**, 917 (1994).

[27] D. Arnold and E. Cartier, Phys. Rev. B **46**, 15 102 (1992).

[28] D. Arnold, E. Cartier, and D. J. DiMaria, Phys. Rev. A **45**, 1477 (1992).

[29] D. von der Linde and H. Schüler, J. Opt. Soc. Am. B (to be published).

[30] P. Audebert, Ph. Daguzan, A. Dos Santos, J. C. Geindre, S. Guizard, G. Hamoniaux, K. Krastev, P. Martin, G. Petite, and A. Antonetti, Phys. Rev. Lett. **73**, 1990 (1994).

[31] B. C. Stuart, S. Herman, and M. D. Perry, IEEE J. Quantum Electron. **QE-31**, 528 (1995).

[32] M. D. Perry, T. Ditmire, and B. C. Stuart, Opt. Lett. **19**, 2149 (1995).

[33] F. Salin, P. Georges, G. Roger, and A. Brun, Appl. Opt. **26**, 4528 (1987).

[34] T. Ditmire, H. Nguyen, and M. D. Perry, J. Opt. Soc. Am. B **11**, 580 (1994).

[35] X. A. Shen, S. C. Jones, and P. Braunlich, Phys. Rev. Lett. **62**, 2711 (1989).

[36] D. Milam, Appl. Opt. **16**, 1204 (1977).

[37] B. K. Ridley, *Quantum Processes in Semiconductors* (Clarendon, Oxford, 1993), pp. 276–278.

[38] L. V. Keldysh, Zh. Eksp. Teor. Fiz. **47**, 1945 (1964) [Sov. Phys. JETP **20**, 1307 (1965)].

[39] M. D. Perry, Ph.D. thesis, University of California, Berkeley, 1987.

[40] M. V. Ammosov, N. B. Delone, and V. P. Krainov, Zh. Eksp. Teor. Fiz. **91**, 2008 (1986) [Sov. Phys. JETP **64**, 1191 (1986)].